Nuclear Materials and Energy 39 (2024) 101656

Contents lists available at ScienceDirect

Nuclear Materials and Energy

journal homepage: www.elsevier.com/locate/nme

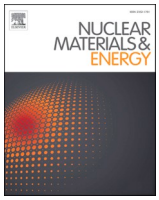

Deuterium retention in tungsten co-deposits with neon and argon inclusions

V. Tiron [a], M.A. Ciolan [a], G. Bulai [b], I. Burducea [c], D. Iancu [c,d], J. Julin [e], M. Kivekäs [e], C. Costin [f,*]

[a] Research Center on Advanced Materials and Technologies, Department of Exact and Natural Sciences, Institute of Interdisciplinary Research, Alexandru Ioan Cuza University of Iasi 700506 Iasi, Romania
[b] Integrated Center of Environmental Science Studies in the North-Eastern Development Region (CERNESIM), Department of Exact and Natural Sciences, Institute of Interdisciplinary Research, Alexandru Ioan Cuza University of Iasi 700506 Iasi, Romania
[c] "Horia Hulubei" National Institute for Research & Development in Physics and Nuclear Engineering, 077125 Magurele, Romania
[d] Faculty of Physics, University of Bucharest 077125 Magurele, Romania
[e] Department of Physics, University of Jyväskylä FI-40014 University of Jyväskylä, Finland
[f] Faculty of Physics, Alexandru Ioan Cuza University of Iasi 700506 Iasi, Romania

ARTICLE INFO

Keywords:
deuterium retention
tungsten co-deposition
neon and argon seeding impurities
bipolar HiPIMS

ABSTRACT

Deuterium (D) retention in tungsten (W) co-deposited layers, in the presence of neon (Ne) and argon (Ar), was investigated using the bipolar High Power Impulse Magnetron Sputtering (BP-HiPIMS) technique. The deposited layers have a polycrystalline structure, with a preferential growth of W(1 1 0) phase. The concentration of D and noble gases (Ne and Ar) is almost constant throughout the depth of the layers. In a D_2-Ar discharge, the deposited layers exhibit compressive stress, indicating that Ar is mostly incorporated into the interstitial sites of the W crystal lattice. D retention increases when Ne is added in the discharge, especially when the deposited layer is bombarded with highly energetic ions. Low energy Ne ions (below the W damaging threshold) induce compressive stress, indicating that Ne atoms occupy interstitial sites in the W crystal lattice. High energy Ne ions induce tensile stress, a sign that Ne is trapped in the grain boundaries as inert-gas-vacancy defects, leading to a grain-boundary relaxation. In the presence of Ne, the ion acceleration towards the layer from 0 V to 300 V results in an increase of the D content of about three times, from 3.2 at.% to 8.6 at.%.

1. Introduction

In 2013, the decision was made that the future experimental fusion reactor ITER would operate with a full-W divertor. Approximately at the same time, an early assessment of the plasma-wall interaction (PWI) physics issues for this new design was published in [1], being later completed with new findings and contributions from the fusion scientific community [2]. A critical issue in the operation of ITER is the tritium (T) inventory build-up in the vessel, which must be limited for safety reasons [3]. The interaction between the fusion plasma and walls/divertor leads, among others, to the retention of the nuclear fuel (D, T), reaction product (He) and seeding impurities (Ne, Ar) in the material of the plasma-facing components (PFCs) [4–7]. The fuelling efficiency and safety of the fusion reactor could be drastically affected by the nuclear fuel accumulation into the PFCs material [3]. On one hand, the fuel retained in the walls/divertor material is lost for the fusion process, and, on the other hand, the radioactive tritium can diffuse through the whole bulk material of the PFCs and contaminate outer parts of the reactor if entering in contact with the coolant [8]. Therefore, the tritium inventory in W PFCs represents one of the most important and complex issues to be addressed in order to ensure the viability and reliability of fusion reactors.

The main processes leading to nuclear fuel retention are implantation and co-deposition with eroded material [3]. The implantation process is based on a direct interaction of the fuel with the surface: the fuel penetrates the surface, the fixation mechanism being trapping or diffusion. For example, the trapping process consists of fuel immobilization in lattice defects (such as impurities, vacancies, dislocations, voids, etc., which are predominantly located in grain boundaries) or in interstitial defects (impurity atoms) [8]. The co-deposition can be seen as a distinct phase of a three-step process: the erosion of the PFCs material under plasma particles bombardment, the migration of the eroded material within the reactor and the incorporation of the fuel material in the re-deposited eroded material. With respect to the localization of the erosion/re-deposition processes, the main wall and the outer divertor are under net erosion, while the inner divertor is a net deposition area

* Corresponding author.
E-mail address: claudiu.costin@uaic.ro (C. Costin).

https://doi.org/10.1016/j.nme.2024.101656
Received 21 February 2024; Received in revised form 12 April 2024; Accepted 16 April 2024
Available online 17 April 2024

[3].

The mechanisms of fuel retention are influenced by various process parameters like the surface temperature [3,5,9,10] and morphology [9,11], plasma composition [4–8,12], as well as ion energy [5,9], flux [10,11] and fluence [3,4,9] of the plasma particles towards the PFCs. Plasma composition is a relevant factor for fuel retention when the nuclear fusion plasma contains seeded impurities, like Ar and/or Ne. In a carbon-free divertor operation scenario, Ar and/or Ne impurities are seeded into the fusion plasma to achieve radiation cooling of the plasma and to suppress the local overheating of the PFCs [13].

The numerous mechanisms of fuel retention and the various factors that influence the process make the study of fuel retention challenging as a whole. Therefore, the fuel retention is usually investigated separately for specific mechanisms and influencing factors [3–11]. For safety reasons, laboratory studies performed on the fuel retention mechanisms have dealt only with D as a substitute for T. For a full-W divertor, it was believed that the main fuel retention process is implantation [3]. However, both experiments [14] and simulations [15] showed that the gross erosion rates in the divertor region can be relatively important, especially during the edge-localized modes (ELMs) [14]. The gross erosion is dominated by the seeded impurities. More than 90 % of the divertor eroded W re-deposits in the same region [14,15], either due to W ions return to the surface as a consequence of the magnetic field presence or due to W screening by the divertor geometry. Although the erosion rates at the wall are predicted to be lower than at the divertor [15], the total amount of eroded material is significant because of the large wall area. This material will partly end up and deposit in the divertor region. Thus, the fuel retention by co-deposition might compete the implantation process.

Deuterium implantation in W was mainly studied by exposing a W target (either bulk or reference coatings) to impurity seeded deuterium plasma in linear magnetized plasma devices, such as PSI-2, PISCES-A, Magnum-PSI, Pilot-PSI [4,5,7,8,10,11], but other types of laboratory plasmas were used as well [9,12]. Regarding the co-deposition process, both erosion and deposition were investigated in fusion devices, either experimentally [3,6,14] or numerically [3,15]. The influence of different characteristics of plasma, eroded material and substrate on the co-deposition was mainly studied in laboratory facilities, in linear machines [16,17] or magnetron sputtering devices [16–19]. The magnetron sputtering/deposition process is not employed as a substitute for the co-deposition in tokamak, but as a versatile tool for producing thin layers (films) with gas inclusions. It has the advantage of simultaneously producing all three steps of the co-deposition process: erosion, migration and deposition. In a typical magnetron discharge, the cathode (also known as target) is sputtered (eroded) by highly energetic ions, while the sputtered material migrates and deposits on a substrate.

A recently developed magnetron operation mode is the bipolar High Power Impulse Magnetron Sputtering (BP-HiPIMS) [20], which is capable to mimic particular aspects of the plasma-wall-interaction under fusion devices relevant conditions. Thus, the instantaneous power density applied on the HiPIMS cathode [21] is comparable to the steady-state heat fluxes in the ITER divertor region (~10 MW/m^2) [2], while the ion energy range measured at the substrate of a BP-HiPIMS plasma [20] covers the range of ion impact energy in the ITER divertor region. The HiPIMS operation mode offers the advantage of a high ionization degree of the sputtered material [22]. Moreover, the process parameters like plasma composition, ion energy and flux are much easier to control in a BP-HiPIMS device, making it versatile for the study of plasma-wall interaction. Therefore, the BP-HiPIMS offers a favourable environment to investigate the deposition of W layers with inclusions of fuel (D) and impurities (Ar and Ne), using a W target and D_2-Ne-Ar gas mixture plasma as ion source. In such a plasma environment, the incident energy of the ions interacting with a surface (here, the interacting surface is the substrate) is independently controlled by the amplitude of the positive voltage (U_+), while the average ion flux by the duration of the negative pulse (τ_-) and the pulse repetition frequency [23]. Although the BP-HiPIMS plasma device cannot fully mimic the conditions in a tokamak, this deposition technique has already been proven to be a good tool for the research of noble gas retention in W-based co-deposited layers. It was shown that the BP-HiPIMS technique allows controlling the inclusion of seeded impurities like Ar and Ne in W reference coatings *via* the ion energy and average flux to the substrate [23]. Also, the HiPIMS technique was used to produce Be-W [24] or Be [25] co-deposited layers containing D areal concentrations comparable to JET-ILW.

As a complement to the previous work [23], this study investigates the D retention in W co-deposited layers, in the presence of Ar and Ne. Two batches of reference samples were synthesized: W sputtered in D_2-Ne-Ar gas mixture and W sputtered only in D_2-Ar gas mixture. Time-of-Flight Elastic Recoil Detection Analysis (ToF-ERDA) was employed for D, Ne, Ar and other elemental impurity quantification and depth profiling, while Scanning Electron Microscopy (SEM) and X-Ray Diffraction (XRD) were used to investigate the influence of plasma parameters on the microstructure and morphology of the W co-deposited layers.

2. Experimental details

W thin layers with gas inclusions were produced in a magnetron sputtering facility operated in BP-HiPIMS mode. The magnetron cathode, which includes a W target of 50 mm in diameter and 3 mm thickness, is placed on the axis of a cylindrical vacuum vessel of 400 mm in diameter and 400 mm height. The experimental set-up is shown in [23] and more technical details can be found in [26]. The base pressure in the vacuum chamber is lower than 10^{-4} Pa. The working pressure was 1 Pa, obtained by injecting the gas mixture at constant flow rates, in two gas combinations: D_2/Ne/Ar of 10/10/10 sccm and D_2/Ar of 10/20 sccm. The D_2 partial pressure was 0.12 Pa in both cases.

The gas content in the deposited samples was modified by adjusting the amplitude of the positive pulse and the width of the negative pulse, while preserving an average power of approximately 100 W *via* the pulse repetition frequency. The negative pulse amplitude (U_-) was kept constant at −800 V, while the positive pulse amplitude (U_+) was varied between 0 V and 300 V. The negative pulse width (τ_-) was tuned from 3 µs to 20 µs, while the positive pulse width (τ_+) was kept constant at 50 µs. In all experiments, the positive pulse was applied right after the negative HiPIMS pulse, without delay. Typical time evolution of the discharge voltage, discharge current and plasma potential measured at the substrate position during BP-HiPIMS of a W target in D_2-Ne-Ar gas mixture are shown in Fig. 1. The plasma potential was measured with an

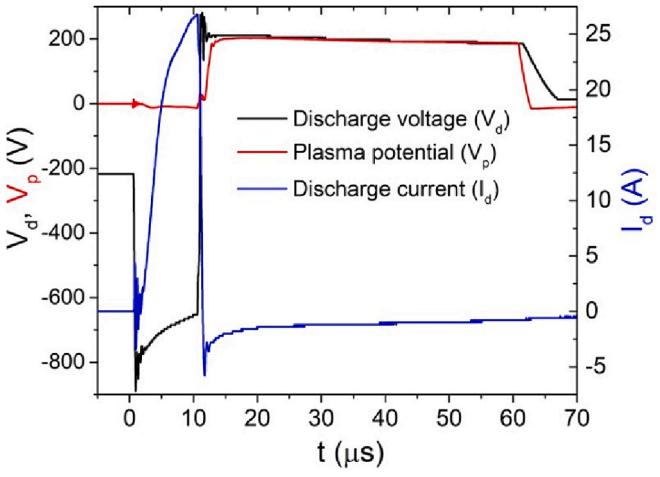

Fig. 1. Typical time evolution of the discharge voltage (V_d), discharge current (I_d) and plasma potential at the substrate position (V_p) during bipolar HiPIMS of a W target in D_2-Ne-Ar gas mixture.

emissive probe [23]. The match between the discharge voltage and plasma potential during the positive pulse highlights the benefit of the BP-HiPIMS in precise control of ion energy. Concerning the average ion flux to the substrate, the ion fluence per pulse increases with the negative pulse width. However, preserving a constant average operating power requires diminishing the pulse repetition frequency when increasing the pulse width. The combined effect of increasing the pulse width and decreasing the repetition frequency results in a decrease of the average ion flux to the substrate, as it was shown for a Ne-Ar discharge [23]. The same behaviour is also valid for a D_2-Ne-Ar discharge, the average ion flux decreasing by less than a factor of two when the negative pulse width increases from 3 μs to 20 μs.

The thin layers were deposited on grounded graphite wafers (10 × 15 mm^2), mechanically polished prior to deposition. Carbon was chosen due to its current use as a PFC material and to ensure a clear distinction between the deposited material and substrate which, in certain cases, can be useful for the film analysis methods (ERDA and XRD). During the deposition process, the substrate temperature increased due to energetic electron and ion bombardment, as well as plasma and target radiation, but it didn't exceed 70 °C, as measured by a thermocouple probe. The deposition time was approximately 1 h for all layers. Post deposition, the content of atomic D, Ne and Ar trapped into the deposited layers and depth profiles were measured by ToF-ERDA using a 13.6 MeV $^{63}Cu^{7+}$ ion beam [27]. The angle between the sample normal and the incoming beam was 70°, while the scattering angle was 40.6°. The analysed area was approximately 3 mm × 3 mm. At the time of ERDA analysis, few samples exhibited cracks and pinholes, leaving the graphite wafer partly uncovered. Therefore, carbon (C) was identified in the ERDA spectra of those samples. As C originates from the substrate, its content in all deposited layers was considered zero when calculating the elemental composition. The concentrations of D, Ne, Ar and W were assumed to sum to 100 %. However, it is unknown how much the D, Ne and Ar results are affected by the C presence. All samples were fully covered after deposition, the cracks appearing in time due to the significant stress induced in the layers, as it will be further discussed.

Layer thickness and morphology were obtained from SEM images. Layer structure was investigated by XRD. The highest peak in all XRD patterns corresponds to W(1 1 0) diffraction plane. The differences in W (1 1 0) peak positions were noticeable enough so that XRD data processing allowed obtaining information about the average crystallite size (L), inter-planar distance (d), lattice parameter (a) and residual strain ($\varepsilon_\perp$). The average crystallite size (L) was estimated from the W(1 1 0) diffraction peak's width, using Scherrer's equation [28]. To quantify the film stress, strain calculations were performed in the direction perpendicular to the film surface based on the inter-planar distance (d – lattice spacing) corresponding to W(1 1 0) diffraction plane. The residual strain ($\varepsilon_\perp$) was calculated as:

$$\varepsilon_\perp = \left(d_{[110]} - d_{0[110]}\right)/d_{0[110]} \quad (1)$$

where $d_{[1\,1\,0]}$ is the stressed crystal lattice spacing and $d_{0[1\,1\,0]}$ is the stress-free crystal lattice spacing for pure W ($d_{0[1\,1\,0]} = 2.238$ Å).

3. Results

3.1. Elemental composition

A typical ToF-ERDA depth profile is shown in Fig. 2. The experimental ERDA data is directly converted into depth profiles using routines from Potku software [29]. Fig. 2 shows that the elemental composition is roughly the same in the depth of the co-deposited layer. Ar quantification suffers from background in the two-dimensional ToF-E histograms due to scattering of incident Cu beam and a background reduction was performed for this element. Noticeable oxygen impurity is detected at the surface of the layer and much less deeper in the film. The origin of oxygen in the depth of layer is the residual oxygen gas and water vapours adsorbed on the walls of the sputtering device, while oxygen detected at the surface of the layer is due to native oxidation of the W co-deposited layer during its storage in environmental conditions.

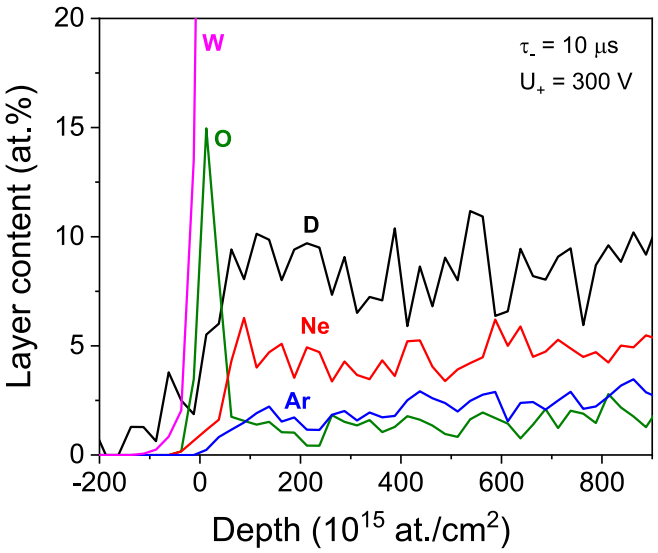

Fig. 2. ERDA depth profile (D_2-Ne-Ar plasma, $\tau_- = 10$ μs, $U_+ = 300$ V).

The ToF-ERDA results show that the atomic D content in the films is the highest among the three gases in the mixture for all investigated conditions (Fig. 3). The retention of the three gases in the co-deposited layers increases gradually by increasing the ion energy to the substrate *via* the positive pulse voltage (Fig. 3(a)). A particular result was found at $U_+ = 100$ V, where the D content deviates from a monotonically increasing dependence on ion energy. For this sample, the C content detected in the ERDA spectrum was significant. As it was already mentioned, C comes from the substrate through cracks and pinholes in the film. Because the nuclear fuel has a higher retention rate in graphite than in W [3], a fraction of the detected D could originate from the substrate as well. As ERDA measurements don't discriminate between the D in the film and substrate, this result has to be considered with caution, as it may overestimate the concentration of D in the film.

The D content has the strongest dependence on the amplitude of the positive pulse (*i.e.* ion energy), increasing from 3.2 at.% to 8.6 at.%, when U_+ changes from 0 V to 300 V, respectively. The content of Ar is mostly constant around 0.6 at.%, significantly increasing to 1.6 at.% only at $U_+ = 300$ V. The content of Ne is in between D and Ar, gaining a factor of two with the increase of U_+.

Fig. 3(b) shows that neither D nor Ne or Ar retention have a significant dependence on the negative pulse width. In our previous paper [23], we showed that when only Ar and Ne gases were used in the discharge, both Ar and Ne concentrations in the films decreased with the increase of the negative pulse width, due to the decrease of the average ion flux to the surface.

Ne presence into the discharge was found to have a more important effect on D retention than Ar. With Ne gas in the plasma, the D retention is significantly higher (Fig. 4), both when changing the positive pulse voltage (Fig. 4(a)) and the negative pulse width (Fig. 4(b)). The highest increase of the D retention is obtained at energetic ion bombardment, i. e. at an acceleration voltage $U_+ = 300$ V (Fig. 4(a)).

3.2. Structural properties

The influence of the plasma composition, ion energy and flux on the microstructure of the W co-deposited layers was investigated by XRD analysis. The diffraction patterns show the presence of two peaks, a strong peak positioned at $2\theta \sim 40°$ corresponding to W(1 1 0), and a weak crystallographic signal positioned at $2\theta \sim 73°$ corresponding to W

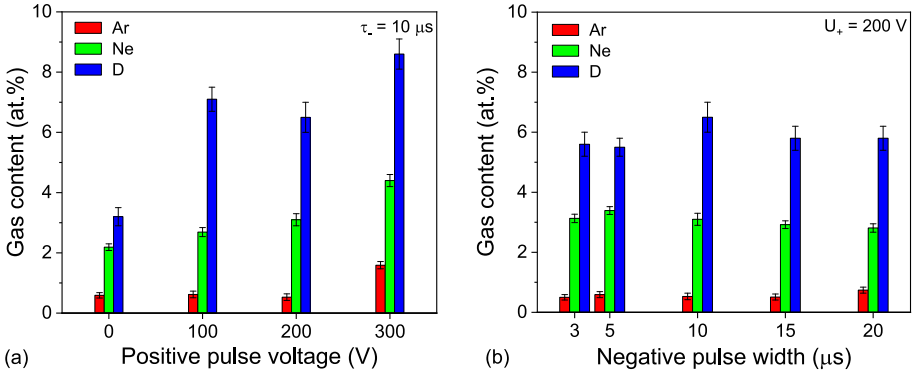

Fig. 3. Influence of the positive pulse voltage (a) and the negative pulse width (b) on Ar, Ne and D content trapped into the W layers (D_2-Ne-Ar plasma).

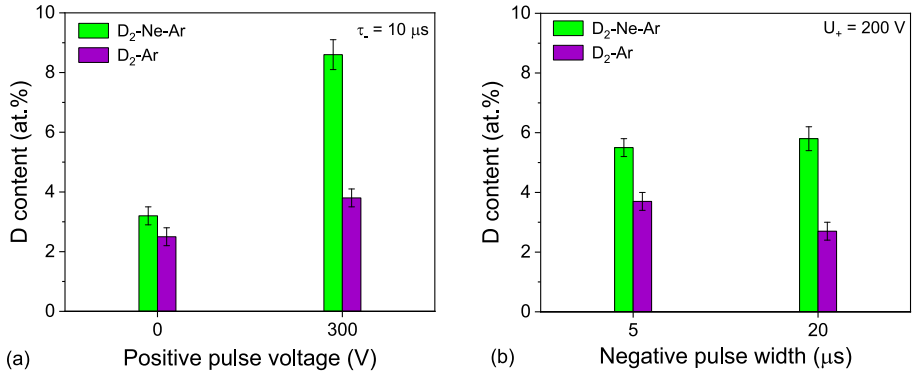

Fig. 4. Influence of the positive pulse voltage (a) and negative pulse width (b) on D retention in the W layers co-deposited in D_2-Ne-Ar and D_2-Ar plasma.

(2 1 1) diffraction planes, both being specific to the body-centred cubic (*bcc*) W phase. The diffraction patterns indicate a polycrystalline structure, with a preferential growth of W(1 1 0) phase. Since the intensity of W(1 1 0) peak is at least ten times higher than W(2 1 1) peak, only XRD diffractograms corresponding to the W(1 1 0) peak are plotted.

Fig. 5 shows the influence of the positive pulse voltage (Fig. 5a) and negative pulse duration (Fig. 5b) on the XRD patterns of the deposited layers. The intensity of W(1 1 0) peaks shows that the crystalline order of W co-deposited layer is significantly weakened when Ne is added in the sputtering gas mixture: the diffraction peaks are smaller for D_2-Ne-Ar plasma than for D_2-Ar plasma. Also, the crystalline order is weaker al low positive pulse voltages or short negative pulses.

In addition, it was noticed that the diffraction peaks of the W co-deposited layers are shifted to smaller angles with respect to pure W ($2\theta = 40.26°$) in the case of D_2-Ar plasma, and to larger angles in the case of D_2-Ne-Ar plasma, except for $U_+ = 0$ V. The shift of the diffraction peak to smaller angles indicates that the inter-planar distance between the planes nearly parallel to the sample surface is larger than in a stress-free film. This means that the lattice is compressed parallel to the film surface and expands perpendicularly to the surface, resulting in a positive residual strain ($\varepsilon_\perp > 0$) which corresponds to a compressive stress. The shift to larger angles indicates an expansion of the lattice parallel to the film surface and a compression perpendicularly to the surface, resulting in a negative residual strain ($\varepsilon_\perp < 0$) which corresponds to a tensile

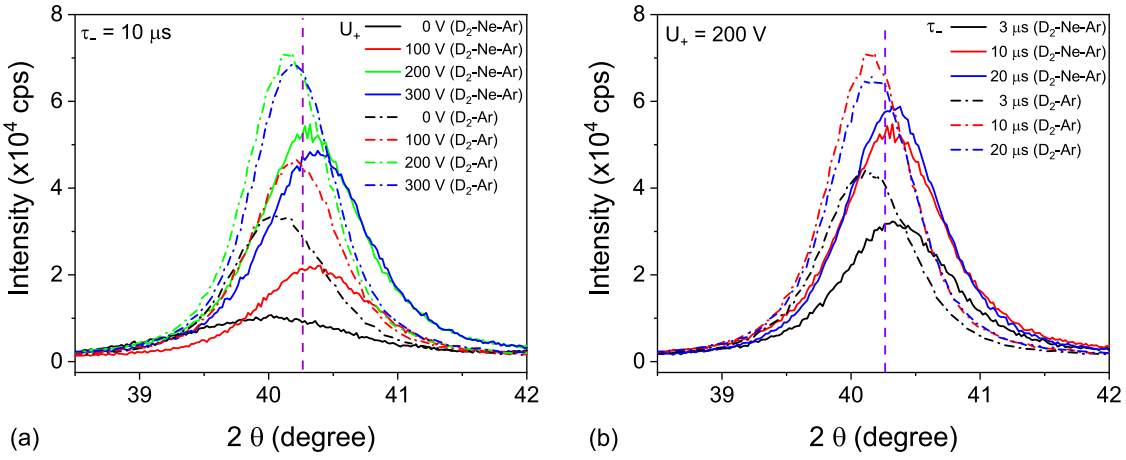

Fig. 5. Influence of the positive pulse voltage (a) and negative pulse width (b) on XRD patterns of W thin films with Ar, Ne and D inclusions. The vertical dash line indicates the position of the W(1 1 0) peak for pure W ($2\theta = 40.26°$).

stress. The average crystallite size (L), inter-planar distance (d), lattice parameter (a), residual strain ($\varepsilon_{\perp}$) resulting from XRD data processing and the layer thickness measured from the SEM images are given in Tables 1 and 2 for all investigated samples. All W thin layers have nanosized crystallites which are larger in D_2-Ar plasma than in D_2-Ne-Ar plasma. The smallest value (5 nm) was found for the W thin films deposited in D_2-Ne-Ar plasma at $U_+ = 0$ V.

Fig. 6 shows the influence of Ne and Ar on the residual strain of the W co-deposited layers. When Ne is present into the discharge and $U_+ = 0$ V, the stress induced in the coatings is compressive, while for higher U_+ values a tensile stress is induced. Without Ne into the discharge, all coatings exhibit a compressive stress. The lattice parameter (a) of the deposited layers is in line with the residual strain (Tables 1 and 2). It is larger than the pure W lattice parameter ($a = 3.1648$ Å) when the stress is compressive and smaller when the stress is tensile. The layers deposited in D_2-Ar plasma have a larger lattice parameter than those deposited in D_2-Ne-Ar plasma, excepting the sample deposited at $U_+ = 0$ V.

3.3. SEM analysis

The influence of the sputtering gas composition on the morphology of the W co-deposited layers is shown in Fig. 7. The W film deposited in D_2-Ne-Ar plasma (Fig. 7(a)) displays a compact morphology, while the W film deposited in D_2-Ar plasma (Fig. 7(b)) displays a textured surface. Most probable, the textured surface is due to the compressive stress induced in the coatings.

The influence of Ne ion bombardment on the morphology and microstructure of the deposited layers is shown in Fig. 8, which shows cross-sectional and top-view SEM images of W co-deposited layer in D_2-Ne-Ar gas mixture at positive pulse voltage of 0 V (Fig. 8(a)) and 300 V (Fig. 8(b)). The film deposited at $U_+ = 0$ V exhibits a compact granular structure with very small grains homogeneously distributed on its surface, while that deposited at $U_+ = 300$ V shows an etch-like surface morphology. The energetic ion bombardment leads to W re-sputtering and thinner deposited layers. Thus, with the increase of U_+, the film thickness decreases (Table 1). Also, the films are thicker in D_2-Ar than in D_2-Ne-Ar plasma (Tables 1 and 2).

4. Discussion

Fig. 2 reveals a typical characteristic of the co-deposition process: the concentration of gas inclusions into the deposited layer is almost uniform in depth. This finding is relevant for fusion reactors because it shows that the amount of fuel trapped into the PFCs by co-deposition increases with the thickness of the deposited layer. In the case of implantation, the concentration of gas inclusions is maximum in the near surface region and decreases inwards [10,11]. The near surface inclusions can act as a barrier, preventing the fuel retention [30], while the co-deposition process is a continuous source of fuel accumulation in the PFCs.

Table 1
Average crystallite size (L), inter-planar distance (d), lattice parameter (a), residual strain ($\varepsilon_{\perp}$) and film thickness (t) corresponding to co-deposited W-D-Ne-Ar and W-D-Ar films at different positive voltages (U_+) and $\tau_- = 10$ μs.

Gas composition	U_+ (V)	L (±1 nm)	d (±0.003 Å)	a (±0.003 Å)	$\varepsilon_{\perp}$ (±0.0006)	t (nm)
D_2-Ne-Ar	0	5	2.254	3.188	0.0077	750
D_2-Ar	0	10	2.247	3.178	0.0046	800
D_2-Ne-Ar	100	8	2.233	3.158	−0.0019	700
D_2-Ar	100	11	2.242	3.170	0.0020	750
D_2-Ne-Ar	200	9	2.235	3.161	−0.0010	550
D_2-Ar	200	11	2.244	3.174	0.0032	600
D_2-Ne-Ar	300	9	2.232	3.157	−0.0022	500
D_2-Ar	300	11	2.242	3.170	0.0021	550

Table 2
Average crystallite size (L), interplanar distance (d), lattice parameter (a), residual strain ($\varepsilon_{\perp}$) and film thickness (t) corresponding to co-deposited W-D-Ne-Ar and W-D-Ar films at different negative pulse durations (τ_-) and $U_+ = 200$ V.

Gas composition	τ_-(μs)	L (±1 nm)	d (±0.003 Å)	a (±0.003 Å)	$\varepsilon_{\perp}$ (±0.0006)	t (nm)
D_2-Ne-Ar	3	8	2.233	3.159	−0.0017	500
D_2-Ar	3	10	2.246	3.176	0.0037	550
D_2-Ne-Ar	5	9	2.235	3.161	−0.0012	520
D_2-Ar	5	10	2.245	3.175	0.0035	570
D_2-Ne-Ar	10	9	2.235	3.161	−0.0010	550
D_2-Ar	10	11	2.244	3.174	0.0032	600
D_2-Ne-Ar	15	9	2.235	3.161	−0.0009	570
D_2-Ar	15	11	2.243	3.172	0.0026	620
D_2-Ne-Ar	20	9	2.234	3.160	−0.0013	570
D_2-Ar	20	11	2.243	3.173	0.0027	620

Fig. 3(a) shows that the D retention in the co-deposited layers increases with the ion energy to the substrate, in agreement with previous reports [16,17]. In the case of BP-HiPIMS, the energy of the ions bombarding the substrate is regulated by the amplitude of the positive pulse, U_+. Previous measurements on the ion energy distribution function (IEDF) at the substrate showed that, in the absence of the positive pulse ($U_+ = 0$ V), the IEDFs of Ar, D and W exhibit a narrow peak below 10 eV and a less populated tale (with about two orders of magnitude), very short for Ar^+ [20], spread up to 100 eV for W^+ [21] and much wider (~300 eV) for D^+ [31]. When the positive pulse is applied, the low energy peak remains almost unchanged and the high energy tale of Ar^+ IEDF becomes very wide, with a maximum of about the same order of magnitude as the low energy peak, corresponding to an ion energy gained in the U_+ acceleration voltage [20]. Similar behaviour has been found for the sputtered material, with the high energy maximum slightly less [20] or more [32,33] energetic than eU_+. Therefore, it is reasonable to assume that a large fraction of all ion species (D^+, Ne^+, Ar^+, W^+) will bombard the substrate with an energy around eU_+. The obtained ion impact energy falls within the range of a tokamak divertor ion energy. As it was shown for WEST, the divertor ion impact energy was estimated to be a few times the upstream electron temperature, corresponding well to the upstream ion energy measured in the scrape-off-layer (SOL) region [34].

Regarding the dependence of the D retention on the ion flux to the substrate, *via* the negative pulse width (Fig. 3(b)), a limitation of the experiment is the lack of information on the partial fluxes of D^+, Ne^+, Ar^+ and W^+. The total ion flux to the substrate was estimated from probe measurements [23], obtaining an instantaneous flux of about 10^{21} $m^{-2}s^{-1}$ during the pulse and 150–250 times lower average flux. Previous measurements found comparable D^+ and W^+ partial fluxes in a magnetron discharge [31], while in the divertor region of WEST tokamak the D^+ flux (~10^{22} $m^{-2}s^{-1}$) is a few orders of magnitude larger than the W^+ flux (~10^{19} $m^{-2}s^{-1}$) [34]. All these fluxes are much smaller than those foreseen for ITER (~10^{24} $m^{-2}s^{-1}$) [35]. Due to the lack of information on partial ion fluxes to the substrate, an alternative reading of Fig. 3(b) is the dependence of the gas content in the deposited layers on the W deposition rate. The film thickness in Table 2 indicates that the W deposition rate increases with the negative pulse width. Unlike previous studies that reported a decrease of the D retention with the increase of the W deposition rate [16,17], in our experiment the dependence is not significant.

Comparing the results in Fig. 3 with the case when only Ne and Ar gases were used [23], it appears that D replaces part of the Ar in the deposited layers. In [23], a gas mixture in equal parts of Ne and Ar generated co-deposited layers with almost the same concentration of Ne and Ar, which had the same dependence on U_+ (ion energy). Of the two noble gases, only Ne has a similar dependence on U_+ in the two experiments. The measured Ne concentrations are not the same in the two

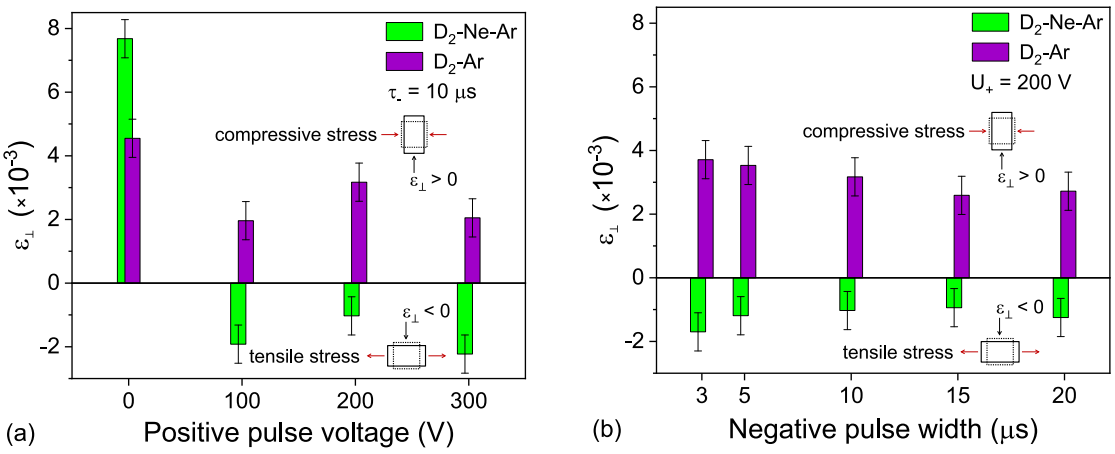

Fig. 6. Influence of the positive pulse voltage (a) and negative pulse width (b) on the residual strain of W thin films co-deposited in D_2-Ne-Ar and D_2-Ar plasma.

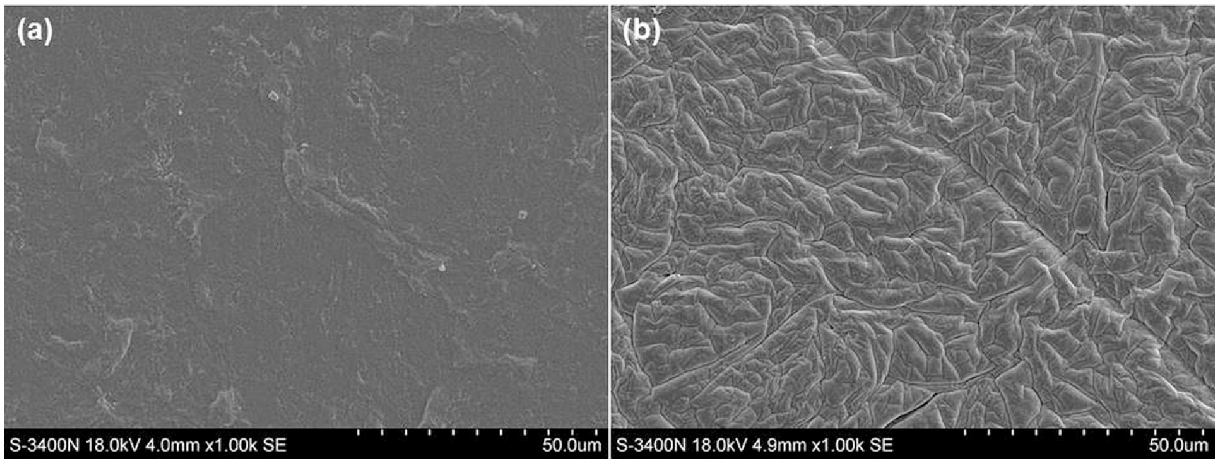

Fig. 7. SEM images of W co-deposited layer in D_2-Ne-Ar (a) and D_2-Ar plasma (b). ($\tau_- = 10$ μs, $U_+ = 200$ V).

experiments, but this cannot be attributed only to the D presence since the detection methods were different: Non-Rutherford Backscattering Spectrometry (NRBS) in [23] and ToF-ERDA here. Previous experiments showed that different methods applied to the same samples can deliver quite different results [5,9]. When D is present into the discharge (Fig. 3), Ar concentration in the film decreases with respect to [23] and the average of D and Ar concentrations is roughly the concentration of Ne. So, D not only replaces Ar in the co-deposited layers, but its concentration is significantly higher than that of Ne and Ar.

As Fig. 4 shows, Ne presence into the discharge has a bigger influence than Ar on the D retention in the W co-deposited layers. As it was already mentioned, the D_2 partial pressure was the same in both D_2-Ne-Ar and D_2-Ar discharges (0.12 Pa). Therefore, the effect of adding Ne on D retention can be the consequence of two phenomena: (*i*) a change in the plasma composition when Ne is present into the discharge resulting in a higher abundance of D ions and (*ii*) a more efficient trapping of D by the Ne-induced defects in the deposited samples [5,7]. The first assumption is related to the higher ionization energy of Ne (21.56 eV) with respect to Ar (15.76 eV). The addition of Ne into the discharge leads to an increase of the electron temperature [36], which changes the ionization rates of the gas mixture components, contributing to the increase of D ions density.

The second assumption is based on the idea that inert gas impurities can increase the D retention if their energies are high enough to produce trapping sites by ion-induced damages [37]. As it was mentioned in the Introduction, the origin of the different trapping sites can be lattice defects, mostly located in grain boundaries, or interstitial defects [8], which can be induced by different kinds of particle fluxes during the experiment. Previous reports showed that both Ne and Ar atoms act as trapping sites for D when incorporated in W, enhancing the retention [38]. However, the defects they induce in the W lattice are different, as well as their effect on D trapping.

Both Ne and Ar atoms can occupy vacant sites in the lattice (*via* migration/trap-mutation for low-energy case and elastic collision for high-energy case) or can be trapped as interstitials. In either cases, they serve as trapping centers for hydrogen isotopes in W, as it was demonstrated by simulations [39,40]. The trapping energy of hydrogen isotopes is higher for Ne- than Ar-vacancy, but lower for Ne- than Ar-interstitial [40]. Ne-induced defects seem more efficient on the D retention than the Ar-induced ones for at least two reasons: the penetration depth in W is higher for Ne than for Ar ions at the same energy [41], and the preferential formation of Ne-vacancy than Ne-interstitials.

The higher penetration depth allows Ne atoms to remain in the W growing film, while near-surface Ar atoms are more easily removed due to the continuous bombardment of the film with energetic ions. Therefore, the content of Ne is higher than that of Ar in the deposited films (Fig. 3). Due to the low diffusion energy barrier of Ne in W (0.17 eV) and the extreme high clustering energies of Ne-vacancy complexes in W (>12 eV), Ne atoms are easily trapped by single vacancies or vacancy clusters [7]. In addition, due to strong attractive interactions between two Ne atoms in bulk W, one Ne atom can easily be trapped by the other, leading to Ne cluster if there are enough Ne atoms nearby [42]. In W, deuterium is highly mobile and accumulates in crystal lattice defects. Due to the larger positive binding energy of D with Ne-vacancies [43]

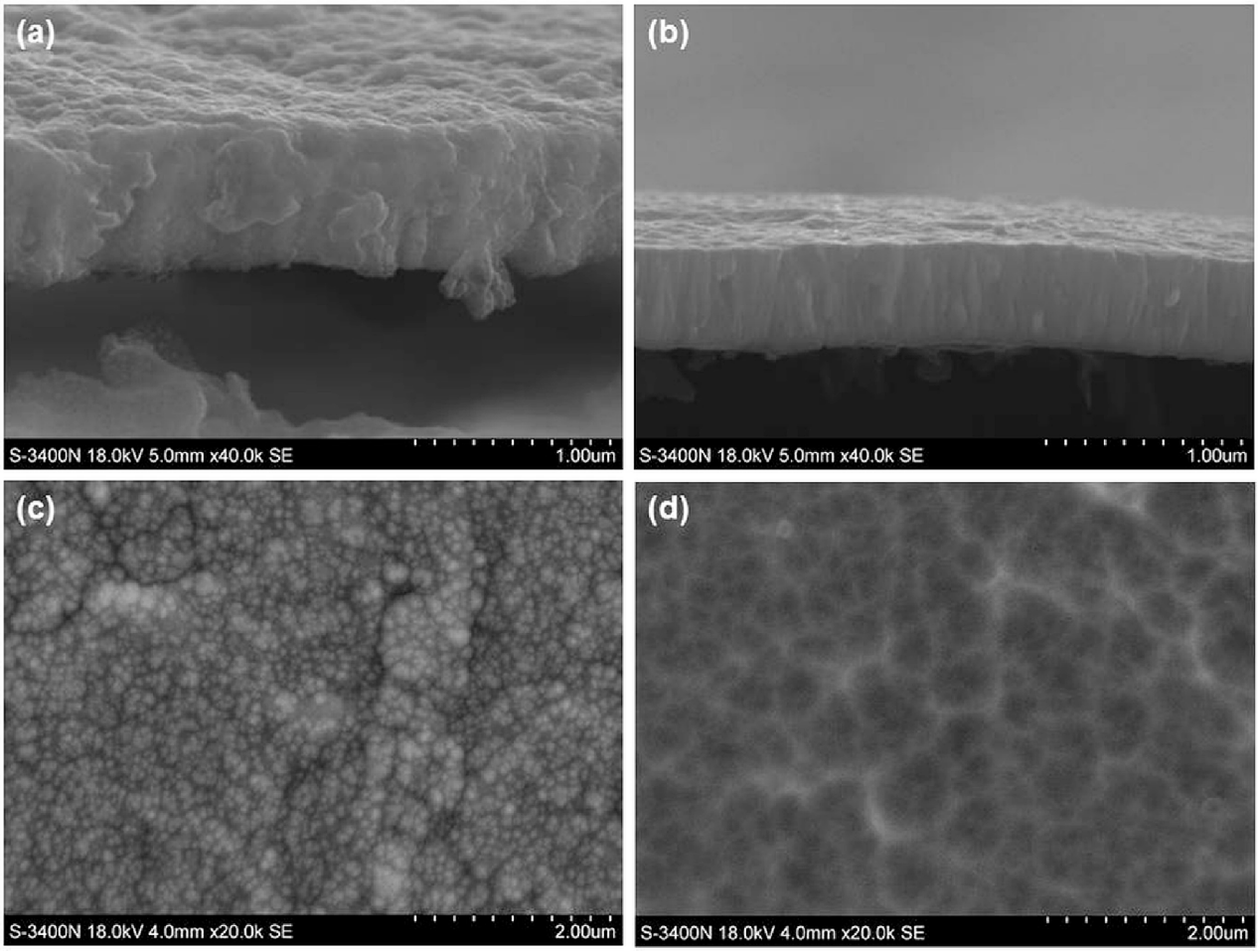

Fig. 8. Cross-sectional (a, b) and top-view (c, d) SEM images of W co-deposited layer in D_2-Ne-Ar gas mixture at positive pulse voltage of 0 V (a, c) and 300 V (b, d). ($\tau_- = 10$ μs).

and due to the continuous incorporation of Ne in the deposited W layers (Fig. 2), Ne impurities act as a getter for D in the entire volume of the deposited layers, enhancing the fuel retention during co-deposition. Thus, Ne role in co-deposition is in contrast to the one played in Ne pre-irradiated PFCs experiments (assimilated to implantation) [30], where Ne atoms act as a barrier that trap D near the surface, reducing the D transport into the bulk and the overall retention.

Furthermore, the XRD analysis showed that Ne inclusions reduce the crystalline order of the W co-deposited layers (Fig. 5), which may also enhance the D retention. Using Thermal Desorption Spectrometry (TDS), Hoen *et al.* [44] showed that the D retention is highly affected by the W film density and crystalline order. A W thin film with low density and amorphous-like structure (with small crystallite size) led to very high deuterium retention with low trapping energies.

Another effect of Ne inclusions is on the residual strain of the co-deposited layers. Fig. 6 shows that when the ions are not accelerated towards the substrate ($U_+ = 0$ V) and the kinetic energy of Ne ions is lower than the W sputtering threshold (38 eV), the stress induced in coatings is compressive, while for a kinetic energy of Ne ions higher than the W sputtering threshold (when the ions are accelerated at $U_+ \geq 100$ V), a tensile stress is induced. Without Ne in the plasma, all layers exhibit compressive stress.

A given material can display either tensile or compressive stress, depending on process specifics and material properties. The thin films deposited using techniques involving energetic particles, such as HiPIMS in Ar atmosphere [21], exhibit predominantly compressive internal stress. This is the case of the films obtained in D_2-Ar plasmas (Fig. 6). One of the main mechanisms underlying this type of stress is the so-called "atomic / ion peening" (lattice distortion caused by energetic particles impacting the forming film) [45,46]. For the films deposited using thermal energy particles, models like grain growth and grain-boundary shrinkage are relatively effective in explaining the tensile stress [47].

In D_2-Ne-Ar plasmas, when the incident Ne ion energy is below the W damaging threshold, Ne atoms mostly occupy interstitial sites in the *bcc* W lattice gaps, leading to a lattice distortion and compressive stress ($U_+ = 0$ V in Fig. 6(a)). When the incident Ne ion energy is beyond the damaging threshold of the W lattice, Ne atoms are mostly introduced in the grain-boundaries as inert-gas-vacancy defects, leading to a crystallite-boundary relaxation, and consequently to a tensile stress. These statements are also supported by the lattice parameter (a) values (Tables 1 and 2). When Ne atoms occupy interstitial sites in the *bcc* W lattice gaps, the lattice parameter (a) is larger than that corresponding to pure W ($a = 3.1648$ Å). When Ne atoms are introduced in the W layer as inert-gas defects in the grain-boundaries, due to their lower mass and volume as compared to W atoms, they induce a grain-boundary relaxation leading to smaller lattice parameter (a).

Based on the data in Tables 1 and 2, it is noticeable that W co-deposited layers in D_2-Ne-Ar plasma have smaller crystalline grains (crystallites) compared to those deposited in D_2-Ar plasma. The same trend was observed in the case of W(211). The model developed by Doljack and Hoffman [48,49], extended by Nix and Clemens [50], elucidates the origin of the tensile stress. During the initial stages of nucleation and island growth on the substrate, the overall average

stresses tend to approach zero, primarily because of the absence of a uniform film. The newly deposited crystallites are drawn together during the deposition process, leading to the merging of crystallites boundaries, often referred to as crystallites coalescence or "zipping". This merging process gives rise to tensile stresses within the films. Because of different crystallographic misalignments, the merging of these islands results in the formation of crystallites boundaries within the film. For adatoms with limited mobility (such as refractory materials), the tensile stress persists even after coalescence, aided by these crystallites boundaries. Conversely, highly mobile adatoms display a secondary phase of compressive growth post coalescence, which is less well-known. According to Nix and Clemens' model, it is suggested that tensile stress should decrease as the crystallites size increases. Our experimental findings align with this explanation, the crystallites size in the compressive stressed films obtained in D_2-Ar plasma being larger than those formed in the tensile stressed films obtained in D_2-Ne-Ar plasma. Thus, it is reasonable to assume that the presence of Ne from the early stages of films formation contributes to grains refinement.

With respect to film thickness, SEM images showed that the films obtained in D_2-Ar plasma are thicker by about 50 nm than those obtained in D_2-Ne-Ar plasma. This is because the W sputtering yield is lower under Ne ion bombardment than Ar [14]. Thus, when Ne is added intro the discharge at the expense of Ar, the W target is less eroded and, consequently, less W is deposited on the substrate (see Tables 1 and 2). Also, the film thickness was found to decrease when increasing the positive pulse voltage. The thickness of the W layers deposited at $U_+ =$ 300 V is about 30 % lower than that of the layers deposited at $U_+ = 0$ V. The thickness loss is consistent with reports of decreased deposition rates observed in bipolar HiPIMS due to film sputtering when operated with high reverse target voltage [20,32,51]. At $U_+ = 300$ V, the D ions also contribute to the film sputtering, knowing that the sputtering threshold for W with D ions is 220 eV [52].

5. Conclusion

D retention in W co-deposited layers was investigated using the bipolar High Power Impulse Magnetron Sputtering (BP-HiPIMS) technique, in the presence of Ne and Ar gases. All three gases were incorporated in the W growing films, almost uniformly throughout the depth of the layers, a typical characteristic of the co-deposition process. D retention was dominant with respect to Ne and Ar, being enhanced in the presence of Ne.

While Ar atoms are mostly incorporated in interstitial sites in the W lattice, generating compressive stressed layers, the Ne atoms locate either in interstitial sites or at the grain boundaries, in the lattice vacancies. Low energy Ne ions (below the W damaging threshold) occupy interstitial sites, inducing compressive stress, similar to Ar. High energy Ne ions are implanted in the grain boundaries, inducing tensile stress. All deposited layers have a polycrystalline structure, with a preferential growth of W(1 1 0) phase. The crystalline order of the deposited layers is significantly weakened when Ne is one of the plasma components. In the presence of Ne, D retention increases significantly with the energy of the ions that reach the growing layer, attaining a concentration of 8.6 at.% for an acceleration voltage of 300 V. The D retention doesn't significantly depend on the W deposition rate.

This study shows that, in contrast to implantation, where D is retained in W mostly at the surface, the co-deposition process leads to D retention within the entire deposited layer. Moreover, the noble gases (Ne and Ar) which are incorporated in the growing films act as trapping sites for D at any step of the deposition process, enhancing the amount of retained fuel. Thus, the noble gases which are used as seeding impurities in fusion reactors may play different roles for the fuel retention in the PFCs, creating a barrier that mitigate the retention during implantation or becoming a fuel getter during co-deposition.

Besides the reported results, further investigations on the influence of other parameters, such as substrate temperature or noble gas fraction in the gas mixture, on the D retention in W co-deposited layers should be considered. Also, the role of the layer's residual stress on the D thermal release could be studied by thermal desorption mass spectrometry.

CRediT authorship contribution statement

V. Tiron: Writing – review & editing, Writing – original draft, Investigation, Formal analysis, Data curation, Conceptualization. **M.A. Ciolan:** Formal analysis. **G. Bulai:** Formal analysis, Data curation. **I. Burducea:** Investigation, Formal analysis, Data curation. **D. Iancu:** Investigation, Formal analysis, Data curation. **J. Julin:** Writing – review & editing, Writing – original draft, Investigation, Formal analysis, Data curation. **M. Kivekäs:** Investigation, Formal analysis, Data curation. **C. Costin:** Writing – review & editing, Writing – original draft, Investigation, Data curation.

Declaration of competing interest

The authors declare that they have no known competing financial interests or personal relationships that could have appeared to influence the work reported in this paper.

Data availability

Data will be made available on request.

Acknowledgments

The research leading to this result has been supported by the RADIATE project under the Grant Agreement 824096 from the EU Research and Innovation programme HORIZON 2020. The contribution of I. B. and D. I. to this work was also supported by two grants of the Romanian Ministry of Research, Innovation and Digitization under projects number PN 19060201 and PDI of IFIN-HH for 2022-2024, 36PFE/2021.

References

[1] R.A. Pitts, S. Carpentier, F. Escourbiac, T. Hirai, V. Komarov, S. Lisgo, A. Kukushkin, A. Loarte, M. Merola, A.S. Naik, A full tungsten divertor for ITER: Physics issues and design status, J. Nucl. Mater. 438 (2013) S48–S56.
[2] R.A. Pitts, X. Bonnin, F. Escourbiac, H. Frerichs, J. Gunn, T. Hirai, A. Kukushkin, E. Kaveeva, M. Miller, D. Moulton, Physics basis for the first ITER tungsten divertor, Nuclear Materials and Energy 20 (2019) 100696.
[3] J. Roth, E. Tsitrone, T. Loarer, V. Philipps, S. Brezinsek, A. Loarte, G.F. Counsell, R. P. Doerner, K. Schmid, O.V. Ogorodnikova, Tritium inventory in ITER plasma-facing materials and tritium removal procedures, Plasma Phys. Controlled Fusion 50 (2008) 103001.
[4] M. Reinhart, A. Kreter, L. Buzi, M. Rasinski, A. Pospieszczyk, B. Unterberg, C. Linsmeier, Influence of plasma impurities on the deuterium retention in tungsten exposed in the linear plasma generator PSI-2, J. Nucl. Mater. 463 (2015) 1021–1024.
[5] A. Kreter, D. Nishijima, R. Doerner, M. Freisinger, C. Linsmeier, Y. Martynova, S. Möller, M. Rasinski, M. Reinhart, A. Terra, Influence of plasma impurities on the fuel retention in tungsten, Nucl. Fusion 59 (2019) 086029.
[6] X. Zhao, C. Sang, Q. Zhou, C. Zhang, Y. Zhang, R. Ding, F. Ding, D. Wang, The erosion of tungsten divertor on EAST during neon impurity seeding in different divertor operation regimes, Plasma Phys. Controlled Fusion 62 (2020) 055015.
[7] Y. Yuan, T. Wang, A. Kreter, M. Reinhart, A. Terra, S. Möeller, L. Cheng, C. Linsmeier, G.-H. Lu, Influence of neon seeding on the deuterium retention and surface modification of ITER-like forged tungsten, Nucl. Fusion 61 (2020) 016007.
[8] M. Reinhart, Influence of impurities on the fuel retention in fusion reactors, PhD Thesis, Forschungszentrum Jülich GmbH Zentralbibliothek, Verlag Jülich, Germany (2015).
[9] A. Manhard, Deuterium inventory in tungsten after plasma exposure: a microstructural survery, PhD Thesis, Augsburg University and Max-Planck-Institute for Plasma Physics in Garching, Germany (2012).
[10] L. Buzi, G. De Temmerman, D. Matveev, M. Reinhart, T. Schwarz-Selinger, M. Rasinski, B. Unterberg, C. Linsmeier, G. Van Oost, Surface modifications and deuterium retention in polycrystalline and single crystal tungsten as a function of particle flux and temperature, J. Nucl. Mater. 495 (2017) 211–219.
[11] L. Buzi, G. De Temmerman, B. Unterberg, M. Reinhart, T. Dittmar, D. Matveev, C. Linsmeier, U. Breuer, A. Kreter, G. Van Oost, Influence of tungsten

microstructure and ion flux on deuterium plasma-induced surface modifications and deuterium retention, J. Nucl. Mater. 463 (2015) 320–324.
[12] M. Ishida, H. Lee, Y. Ueda, The influence of neon or argon impurities on deuterium permeation in tungsten, J. Nucl. Mater. 463 (2015) 1062–1065.
[13] A. Kallenbach, M. Bernert, R. Dux, L. Casali, T. Eich, L. Giannone, A. Herrmann, R. McDermott, A. Mlynek, H. Müller, Impurity seeding for tokamak power exhaust: from present devices via ITER to DEMO, Plasma Phys. Controlled Fusion 55 (2013) 124041.
[14] S. Brezinsek, A. Kirschner, M. Mayer, A. Baron-Wiechec, I. Borodkina, D. Borodin, I. Coffey, J. Coenen, N. den Harder, A. Eksaeva, Erosion, screening, and migration of tungsten in the JET divertor, Nucl. Fusion 59 (2019) 096035.
[15] A. Eksaeva, A. Kirschner, J. Romazanov, S. Brezinsek, C. Linsmeier, F. Maviglia, M. Siccinio, S. Ciattaglia, Predictive 3D modelling of erosion and deposition in ITER with ERO2. 0: from beryllium main wall, tungsten divertor to full-tungsten device, Phys. Scr. 97 (2022) 014001.
[16] G. De Temmerman, R. Doerner, Deuterium retention and release in tungsten co-deposited layers, J. Nucl. Mater. 389 (2009) 479–483.
[17] V.K. Alimov, J. Roth, W. Shu, D. Komarov, K. Isobe, T. Yamanishi, Deuterium trapping in tungsten deposition layers formed by deuterium plasma sputtering, J. Nucl. Mater. 399 (2010) 225–230.
[18] M. Baldwin, M. Simmonds, G. De Temmerman, R. Doerner, Deuterium retention in Be-D co-deposits formed over an ITER relevant parameter space, Phys. Scr. 2020 (2020) 014014.
[19] S. Krat, E. Fefelova, A. Pryshvitsin, Y. Gasparyan, I. Sorokin, V. Efimov, A. Pisarev, Effect of helium presence on tungsten-deuterium co-deposited films, Nuclear Materials and Energy 34 (2023) 101336.
[20] I.-L. Velicu, G.-T. Ianoş, C. Porosnicu, I. Mihăilă, I. Burducea, A. Velea, D. Cristea, D. Munteanu, V. Tiron, Energy-enhanced deposition of copper thin films by bipolar high power impulse magnetron sputtering, Surf. Coat. Technol. 359 (2019) 97–107.
[21] I.-L. Velicu, V. Tiron, C. Porosnicu, I. Burducea, N. Lupu, G. Stoian, G. Popa, D. Munteanu, Enhanced properties of tungsten thin films deposited with a novel HiPIMS approach, Appl. Surf. Sci. 424 (2017) 397–406.
[22] V. Kouznetsov, K. Macak, J.M. Schneider, U. Helmersson, I. Petrov, A novel pulsed magnetron sputter technique utilizing very high target power densities, Surf. Coat. Technol. 122 (1999) 290–293.
[23] V. Tiron, G. Bulai, C. Costin, I.-L. Velicu, P. Dincă, D. Iancu, I. Burducea, Growth and characterization of W thin films with controlled Ne and Ar contents deposited by bipolar HiPIMS, Nuclear Materials and Energy 29 (2021) 101091.
[24] P. Dinca, C. Porosnicu, B. Butoi, I. Jepu, V. Tiron, O. Pompilian, I. Burducea, C. Lungu, I.-L. Velicu, Beryllium-tungsten study on mixed layers obtained by m-HiPIMS/DCMS techniques in a deuterium and nitrogen reactive gas mixture, Surf. Coat. Technol. 321 (2017) 397–402.
[25] M. Zlobinski, G. Sergienko, Y. Martynova, D. Matveev, B. Unterberg, S. Brezinsek, B. Spilker, D. Nicolai, M. Rasinski, S. Möller, Laser-Induced Desorption of co-deposited Deuterium in Beryllium Layers on Tungsten, Nuclear Materials and Energy 19 (2019) 503–509.
[26] V. Tiron, I.-L. Velicu, I. Mihăilă, G. Popa, Deposition rate enhancement in HiPIMS through the control of magnetic field and pulse configuration, Surf. Coat. Technol. 337 (2018) 484–491.
[27] M. Laitinen, M. Rossi, J. Julin, T. Sajavaara, Time-of-flight–Energy spectrometer for elemental depth profiling–Jyväskylä design, Nucl. Instrum. Methods Phys. Res., Sect. B 337 (2014) 55–61.
[28] A. Patterson, The Scherrer formula for X-ray particle size determination, Phys. Rev. 56 (1939) 978.
[29] K. Arstila, J. Julin, M. Laitinen, J. Aalto, T. Konu, S. Kärkkäinen, S. Rahkonen, M. Raunio, J. Itkonen, J.-P. Santanen, Potku-New analysis software for heavy ion elastic recoil detection analysis, Nucl. Instrum. Methods Phys. Res., Sect. B 331 (2014) 34–41.
[30] L. Cheng, G. De Temmerman, P.Z. Van Emmichoven, G. Ji, H.-B. Zhou, B. Wang, Y. Yuan, Y. Zhang, G.-H. Lu, Effect of neon plasma pre-irradiation on surface morphology and deuterium retention of tungsten, J. Nucl. Mater. 463 (2015) 1025–1028.
[31] P. Dinca, V. Tiron, I.-L. Velicu, C. Porosnicu, B. Butoi, A. Velea, E. Grigore, C. Costin, C. Lungu, Negative ion-induced deuterium retention in mixed W-Al layers co-deposited in dual-HiPIMS, Surf. Coat. Technol. 363 (2019) 273–281.
[32] J. Keraudy, R.P.B. Viloan, M.A. Raadu, N. Brenning, D. Lundin, U. Helmersson, Bipolar HiPIMS for tailoring ion energies in thin film deposition, Surf. Coat. Technol. 359 (2019) 433–437.
[33] T. Kozák, A.D. Pajdarová, M. Čada, Z. Hubička, P. Mareš, J. Čapek, Ion energy distributions at substrate in bipolar HiPIMS: effect of positive pulse delay, length and amplitude, Plasma Sources Sci. Technol. 29 (2020) 065003.
[34] Y. Li, N. Fedorczak, G. Xu, Y. Liang, S. Brezinsek, J. Morales, W. Team, Effect of edge ion temperature on the divertor tungsten sputtering in WEST, Nucl. Fusion 63 (2023) 026019.
[35] G. Federici, C.H. Skinner, J.N. Brooks, J.P. Coad, C. Grisolia, A.A. Haasz, A. Hassanein, V. Philipps, C.S. Pitcher, J. Roth, Plasma-material interactions in current tokamaks and their implications for next step fusion reactors, Nucl. Fusion 41 (2001) 1967.
[36] A. Aijaz, K. Sarakinos, D. Lundin, N. Brenning, U. Helmersson, A strategy for increased carbon ionization in magnetron sputtering discharges, Diam. Relat. Mater. 23 (2012) 1–4.
[37] W. Wang, J. Roth, S. Lindig, C. Wu, Blister formation of tungsten due to ion bombardment, J. Nucl. Mater. 299 (2001) 124–131.
[38] L. Cheng, Z. Zhao, G. De Temmerman, Y. Yuan, T. Morgan, L. Guo, B. Wang, Y. Zhang, B. Wang, P. Zhang, Effect of noble gas ion pre-irradiation on deuterium retention in tungsten, Phys. Scr. 2016 (2015) 014001.
[39] X.-S. Kong, J. Hou, X.-Y. Li, X. Wu, C. Liu, J.-L. Chen, G.-N. Luo, First principles study of inert-gas (helium, neon, and argon) interactions with hydrogen in tungsten, J. Nucl. Mater. 487 (2017) 128–134.
[40] Y.-H. Li, H.-B. Zhou, G.-H. Lu, Towards understanding the strong trapping effects of noble gas elements on hydrogen in tungsten, Int. J. Hydrogen Energy 42 (2017) 6902–6917.
[41] M. Yajima, M. Yamagiwa, S. Kajita, N. Ohno, M. Tokitani, A. Takayama, S. Saito, A. M. Ito, H. Nakamura, N. Yoshida, Comparison of damages on tungsten surface exposed to noble gas plasmas, Plasma Sci. Technol 15 (2013) 282.
[42] G. Liu, S. Xiao, H.-B. Zhou, Z. Liu, W. Hu, F. Gao, H. Deng, Effect of neon on the hydrogen behaviors in tungsten: A first-principles study, J. Nucl. Mater. 510 (2018) 492–498.
[43] G.-Y. Huang, N. Juslin, B.D. Wirth, First-principles study of vacancy, interstitial, noble gas atom interstitial and vacancy clusters in bcc-W, Comput. Mater. Sci 123 (2016) 121–130.
[44] D. Dellasega, A. Pezzoli, M. Passoni, A. Kleyn, P.Z. Van Emmichoven, Deuterium retention and surface modifications of nanocrystalline tungsten films exposed to high-flux plasma, J. Nucl. Mater. 463 (2015) 989–992.
[45] R. Daniel, K. Martinschitz, J. Keckes, C. Mitterer, The origin of stresses in magnetron-sputtered thin films with zone T structures, Acta Mater. 58 (2010) 2621–2633.
[46] H. Windischmann, Intrinsic stress in sputter-deposited thin films, Critical Reviews in Solid State and Material Sciences 17 (1992) 547–596.
[47] A.R. Shugurov, A.V. Panin, Mechanisms of stress generation in thin films and coatings, Tech. Phys. 65 (2020) 1881–1904.
[48] F.A. Doljack, R. Hoffman, The origins of stress in thin nickel films, Thin Solid Films 12 (1972) 71–74.
[49] R. Hoffman, Stresses in thin films: The relevance of grain boundaries and impurities, Thin Solid Films 34 (1976) 185–190.
[50] W. Nix, B. Clemens, Crystallite coalescence: A mechanism for intrinsic tensile stresses in thin films, J. Mater. Res. 14 (1999) 3467–3473.
[51] R.P.B. Viloan, U. Helmersson, D. Lundin, Copper thin films deposited using different ion acceleration strategies in HiPIMS, Surf. Coat. Technol. 422 (2021) 127487.
[52] P. Ghendrih, The plasma boundary of magnetic fusion devices, Plasma Phys. Controlled Fusion 43 (2001) 223–224.